Spectrum of Engineering Sciences
ISSN (e) 3007-3138 (p) 3007-312X Volume 3, Issue 10, 2025

COMPARATIVE STRUCTURAL ANALYSIS OF THE HIGHER HIMALAYA, KAGHAN VALLEY, PAKISTAN: INTEGRATING SENTINEL-1 AND ALOS PALSAR SAR DATA WITH GEOLOGICAL FIELD MAPPING

Majid Farooq[1,2], Sohail Wahid[1], Azeem Khan[1,2], Azmat Rasool[2], Zia Ur Rehman Farooqi[2]

[1] *National Center of Excellence in Geology, University of Peshawar, Pakistan*
[2] *Geoscience Advanced Research Laboratories, Geological Survey of Pakistan, Islamabad, Pakistan*

DOI: https://doi.org/10.5281/zenodo.17407204

Keywords
Sentinel-1; ALOS PALSAR; SAR; Kaghan Valley; Himalaya; Structural Mapping; Field Integration; Neotectonics

Article History
Received on 20 Sep 2025
Accepted on 28 Sep 2025
Published on 21 Oct 2025

Corresponding Author: *

Majid Farooq
MajidFarooq415@yahoo.com

Abstract

This study presents an integrated structural analysis of the Higher Himalaya in the Kaghan Valley, Pakistan, utilizing Sentinel-1 C-band and ALOS PALSAR L-band synthetic aperture radar (SAR) data combined with detailed field-based geological mapping. Key tectonic features, including the Main Mantle Thrust (MMT), Main Central Thrust (MCT), and associated folds and back-thrusts, were identified and analyzed. Sentinel-1 (VV, VH) imagery highlighted topographic contrasts and steep structural elements, while ALOS PALSAR (HH, HV) offered superior vegetation penetration, enhancing the visualization of geomorphic offsets and fault scarps. The integration of satellite-derived lineaments with field-mapped structures refined the regional tectonic framework. Comparative analysis indicates that C-band data effectively delineate ridges and fault-controlled drainages, whereas L-band imagery excels in identifying buried or vegetated faults. This combined approach produces a validated structural map that advances understanding of Himalayan tectonic architecture and its neotectonic implications, aligning with recent advancements in SAR applications for landslide and deformation monitoring.

INTRODUCTION

The Himalayas represent one of the most active orogenic systems on Earth, formed by the ongoing collision between the Indian and Eurasian plates (Yin, 2006). Structural mapping of thrusts and associated folds is essential for understanding tectonic evolution and contemporary neotectonic processes (Bilham, 2019). However, the region's steep relief, dense vegetation, and harsh weather often limit direct field observations (Ghosh et al., 2023). Synthetic aperture radar (SAR) remote sensing provides an all-weather, day-night capability for detecting deformation and topographic expressions of structures, making it invaluable for Himalayan studies (Small & Schubert, 2019; Rather & Bukhari, 2025).

This study compares Sentinel-1 (C-band) and ALOS PALSAR (L-band) data to delineate tectonic structures in the Higher Himalaya of the Kaghan Valley, integrating remote sensing outputs with field mapping to enhance accuracy. Recent applications of multi-sensor SAR have demonstrated improved detection of active landslides and subsurface deformations in similar terrains (Liu et al., 2021; Xiong et al., 2017; Oludare et al., 2023). By fusing these datasets, we

aim to refine the tectonic model of the Kaghan Valley, contributing to geo-hazard assessments in the northwestern Himalaya (Ahmed et al., 2023; Karaca et al., 2021).

2. Study Area

The Kaghan Valley, located in the northwestern Himalaya of Pakistan, occupies a tectonically complex sector bounded by the MMT, MCT, and subsidiary splays (Figure 1) (Baig & Lawrence, 1987). The valley exhibits pronounced geomorphic evidence of active deformation, such as triangular facets, offset drainages, shutter ridges, and linear valleys (Shahzad & Gloaguen, 2011). Lithologically, the area comprises metamorphic and igneous rocks of the Higher Himalayan Crystalline Sequence and Lesser Himalayan units (Shami & Baig, 2002).

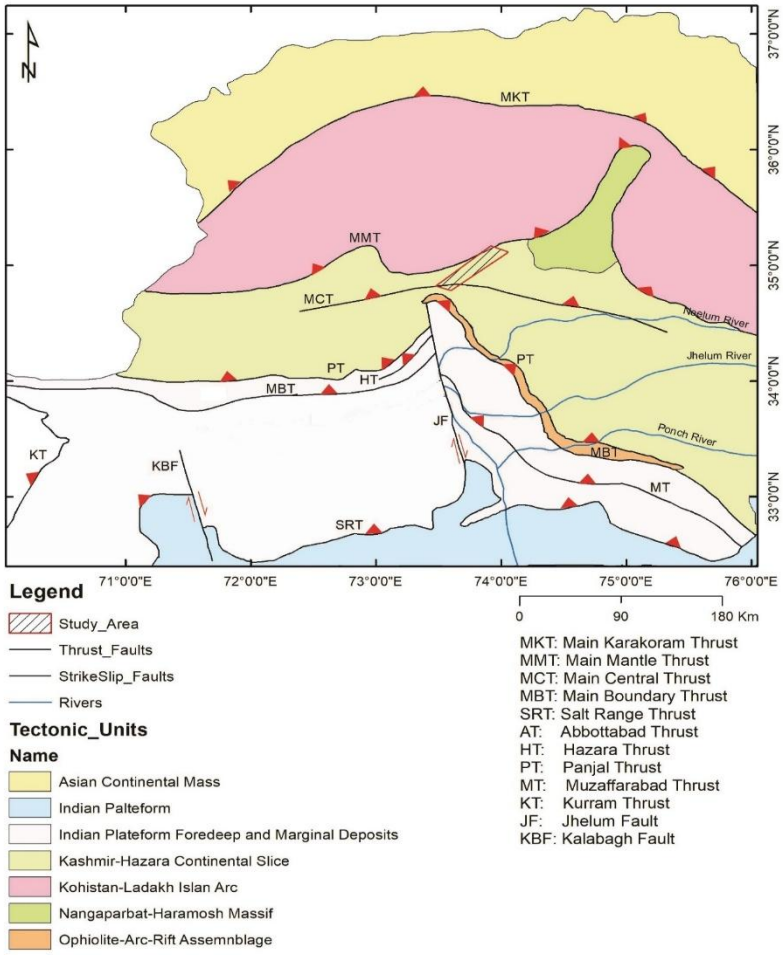

Figure 1: Tectonic map of northwest Himalayas of Pakistan, compiled from Wadia (1928), Latif (1970), Kazmi and Rana (1982), Baig and Lawrence (1987), Shami and Baig (2002), Baig et al. (2010). Rectangle shows the study area.

3. Data and Methods

3.1 Remote Sensing Data Acquisition and Processing

Remote sensing plays a crucial role in identifying topographical and structural features in structural geology (Zeinalov et al., 2000; Ahmadi et al., 2023). Sentinel-1 satellite imagery, along with its by-products (e.g., with and without terrain flattening), aids in identifying regional fault lines through variations in polarization patterns (Saraf et al., 2002; Small & Schubert, 2019). In this study, Sentinel-1 and ALOS PALSAR data were used to analyze topographic and structural features (Figures 3, 4, 5 and 6).

Dual-polarization Sentinel-1 (VV, VH) and ALOS PALSAR (HH, HV) scenes were processed using SNAP and ENVI software. Processing steps included radiometric calibration, terrain correction, and speckle filtering (Huang et al., 2017; Thollard et al., 2021). Terrain flattening was selectively applied to Sentinel-1 imagery, as unflattened data better highlighted reverse and back-thrust faults in complex topography (Abdikan et al., 2016; Zhu et al., 2022). Polarization ratios (VH/VV, HH/HV) were generated to accentuate lithologic and structural contrasts (Bhosle et al., 2009; Ji et al., 2020).

For ALOS PALSAR, two L-band images ("ALPSRP087910680" and "ALPSRP087910690", acquired on 18-09-2007, HH+HV polarization, ascending orbit) were downloaded and interpreted (Shimada et al., 2009; Kwak et al., 2007). The HH band provided high-resolution geomorphology and topography, while HV aided in vegetation and roughness analysis (Zhou et al., 2015; Jiang et al., 2008).

3.2 Field Mapping and Integration

Fieldwork involved measuring fault orientations, fold axes, and geomorphic markers for ground validation (Mahmood et al., 2012; Waheed et al., 2019). Satellite-derived lineaments were overlaid with field data to validate interpretations (Lu et al., 2021; Aoki et al., 2008).

4. Results

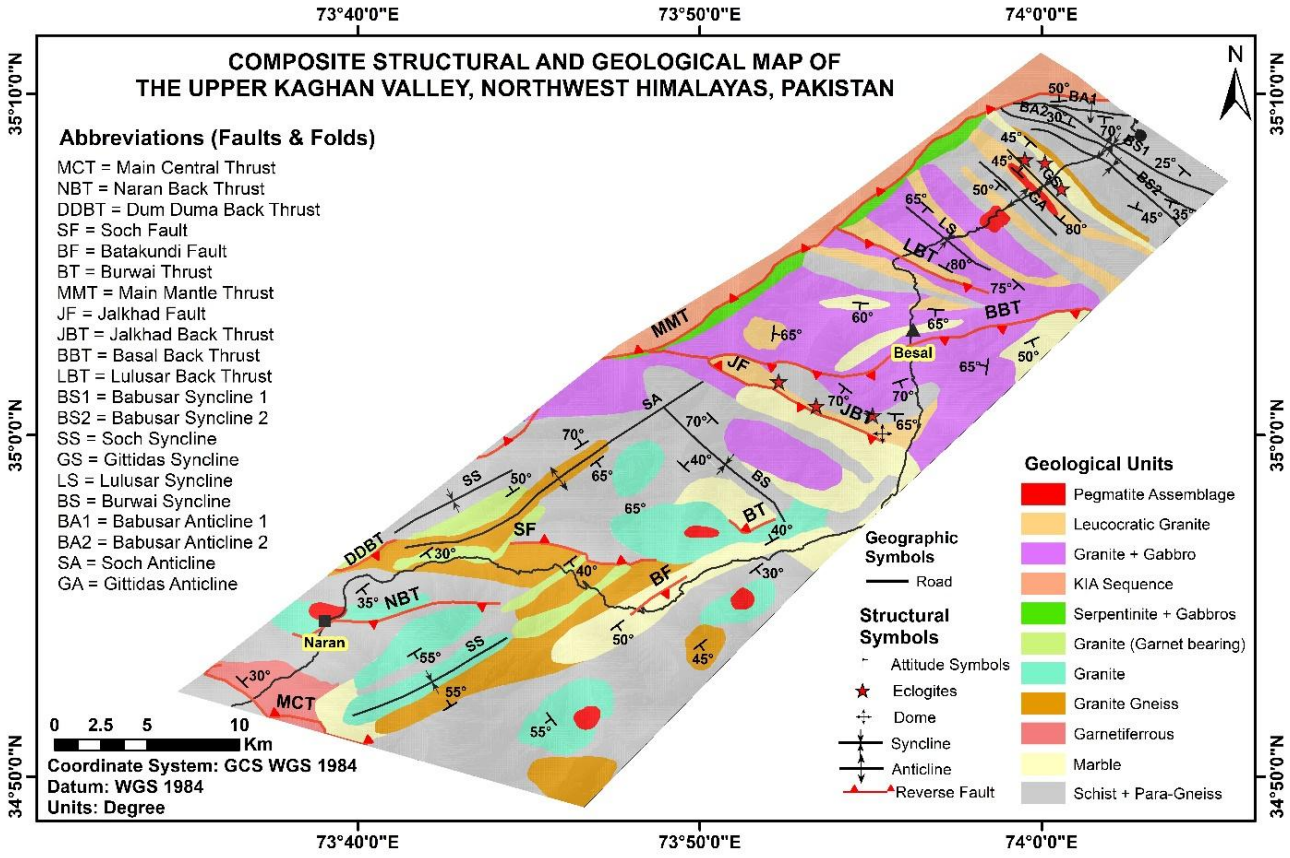

Figure 2: Field-based geological and structural map of the study area.

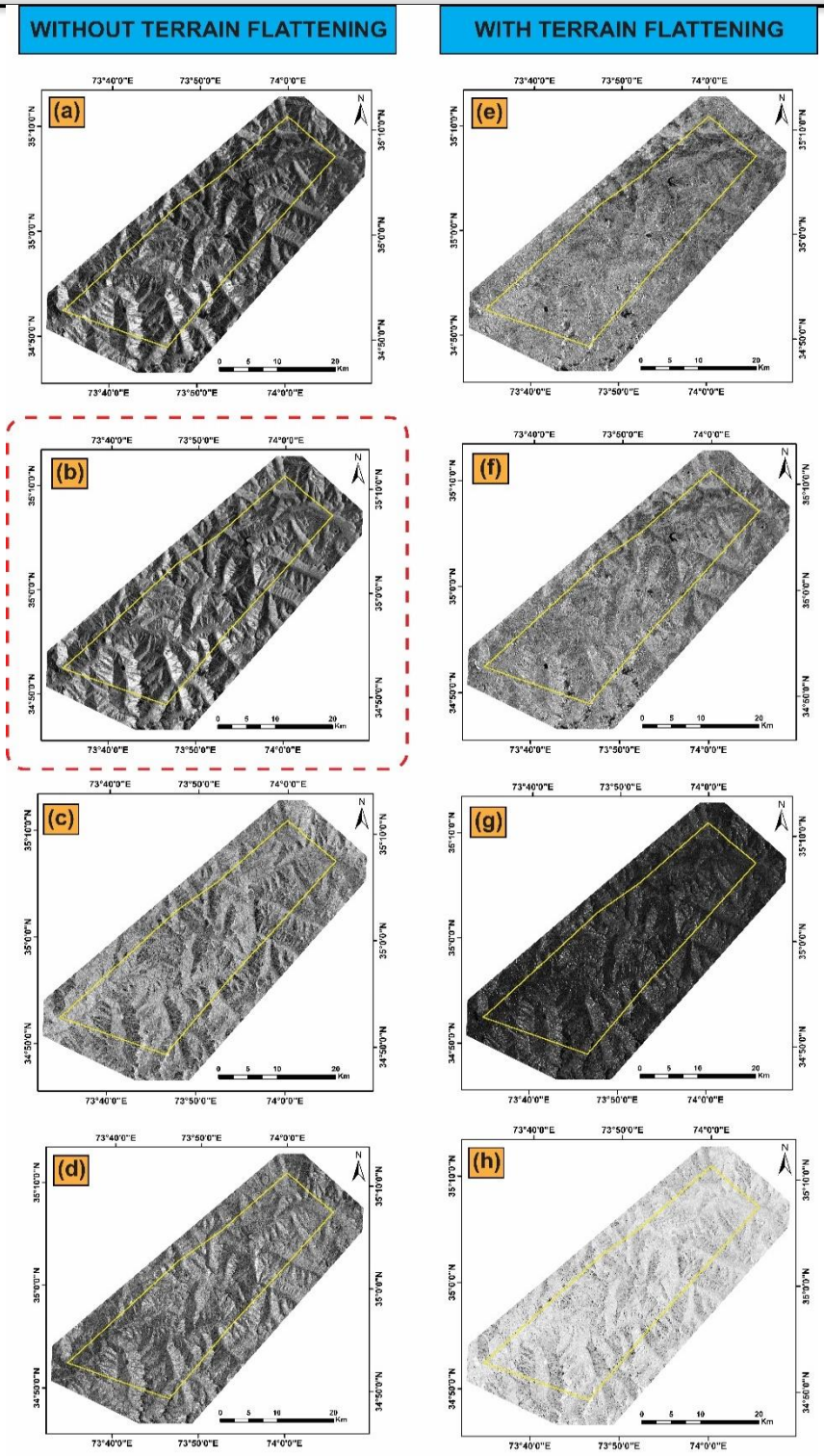

Figure 3: Illustrates the comparison of Sentinel-1 imagery with and without terrain flattening: (a, e) VH polarization; (b, f) VV polarization; (c, g) VH over VV; (d, h) VV over VH (Bhosle et al., 2009).

VV polarization (without terrain flattening) effectively delineated structural features, including major faults and folds, through geomorphic indicators like drainage patterns, topographic

fronts, triangular facets, linear springs, shutter ridges, and fault-controlled ridges and streams (Oguchi et al., 2003; Meixner et al., 2018; EL-Omairi et al., 2024).

4.1 Sentinel-1 Analysis

The MMT, running northeast to southwest, controlled stream patterns (Hu & Zhu, 2022). Similarly, the NBT, BF, and BBT influenced drainage and topography (Weilert & Laó-Dávila, 2023). Higher backscatter in VV polarization defined topographic highs and structural controls (Watson et al., 2022; Huang et al., 2022).

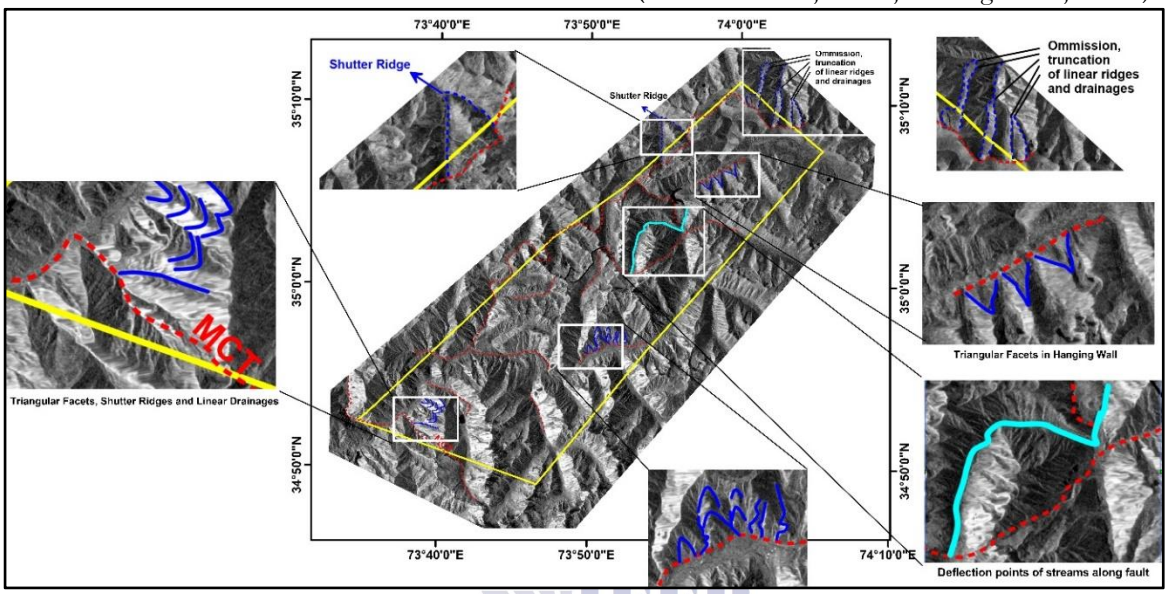

Figure 4: Sentinel-1 satellite imageries with identified structural features.

4.2 ALOS PALSAR Analysis

ALOS PALSAR's L-band provided penetration through vegetation, detecting deformations and displacements (Shimada et al., 2009; Xiong et al., 2017). HH polarization excelled in surface deformation monitoring, topographic mapping, and fault characterization using InSAR techniques (Jiang et al., 2008; Aoki et al., 2008; Lu et al., 2007). HV polarization supported vegetation and soil analysis (Bovenga et al., 2014; Zhang et al., 2019).

Faults were identified based on geomorphic features like river delineations, topographic fronts, shutter ridges, strata truncations, triangular facets, ridge omissions, linear springs, spurs, valleys, uplifted peaks, dilations, and transecting fault sets (Figure 5, 6). The MCT and MMT controlled landslides and topography.

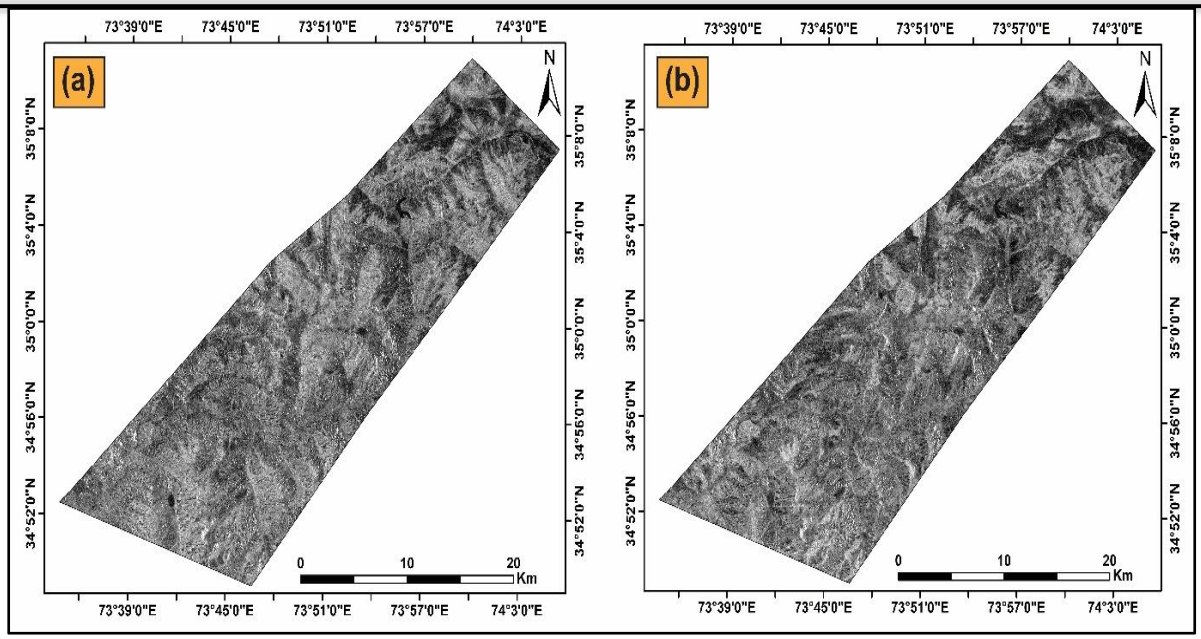

Figure 5: ALOS PALSAR imageries with (a) HH and (b) HV polarizations.

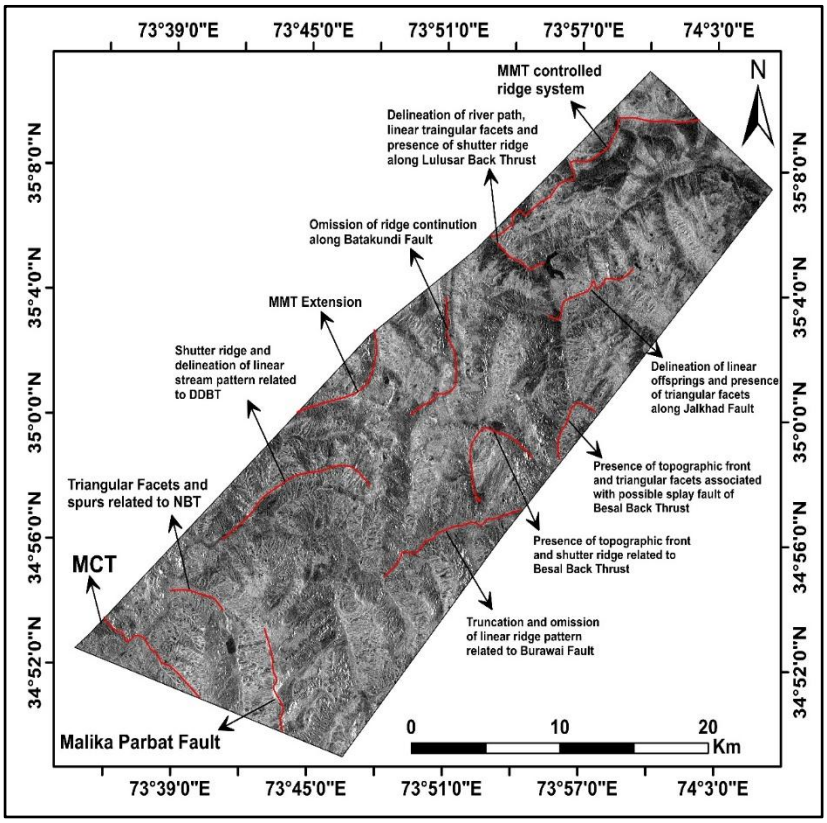

Figure 6: ALOS PALSAR imageries with identified structural features.

4.3 Integrated Interpretation of Structural Features

The integrated interpretation combines satellite-derived lineaments with field data, delineating the MMT, MCT, Kaghan Thrust, and NE–SW-trending back-thrusts and en-échelon folds, confirming the regional thrust architecture (Ghosh et al., 2023; Ahmed et al., 2023).

The integration of satellite-derived lineaments from Sentinel-1 and ALOS PALSAR with field-based geological data provides a comprehensive structural analysis of the Kaghan Valley, delineating key tectonic features such as the Main Mantle Thrust (MMT), Main Central Thrust (MCT), Kaghan Thrust, and northeast–southwest-trending back-thrusts and en-échelon folds (Ghosh et al., 2023; Ahmed et al., 2023). Sentinel-1's VV polarization highlighted fault-controlled ridges and drainage patterns, effectively mapping the MMT and MCT through geomorphic indicators like triangular facets and shutter ridges (Small & Schubert, 2019; Oguchi et al., 2003). ALOS PALSAR's HH polarization penetrated vegetation to reveal buried fault scarps and offset streams, enhancing the detection of back-thrusts and folds (Shimada et al., 2009; Xiong et al., 2017). Field measurements of fault orientations and fold axes validated these findings, confirming the alignment of SAR-derived lineaments with observed structures (Waheed et al., 2019; Mahmood et al., 2012). The resulting structural map (Figure 2) synthesizes these datasets, revealing active deformation and supporting neotectonic assessments in the Higher Himalaya (Liu et al., 2021; Zhao et al., 2022).

5. Discussion

The comparison of C- and L-band datasets reveals that wavelength influences structural visibility. Sentinel-1's C-band is sensitive to slope and roughness, excelling at topographic fronts and ridge alignments (Abdikan et al., 2016; Zhao et al., 2022). ALOS PALSAR's L-band penetrates vegetation, capturing fault signatures beneath cover (Xiong et al., 2017; Ahmadi et al., 2023).

These findings align with prior Himalayan studies (Wadia, 1928; Baig & Lawrence, 1987; Shami & Baig, 2002) and recent remote-sensing analyses (Lu et al., 2021; Oludare et al., 2023; Karaca et al., 2021). Integration with field data validates SAR lineaments coinciding with mapped faults, particularly the MCT and Kaghan Thrust (Mahmood et al., 2013; Waheed et al., 2019). Geomorphic evidence indicates ongoing neotectonic activity (Shahzad & Gloaguen, 2011; Rather & Bukhari, 2025).

The multi-sensor approach is effective for rugged terrains, with implications for hazard assessment (Liu et al., 2021; Ghosh et al., 2023).

5. This methodology provides a framework for tectonic and hazard studies (Ahmed et al., 2023; Oludare et al., 2023).

6. Conclusions

1. Sentinel-1 VV polarization outlines steep ridges and fronts, while ALOS PALSAR HH delineates vegetated structures.

2. Multi-sensor SAR with field mapping yields a comprehensive structural interpretation.

3. The refined map defines the MMT, MCT, back-thrusts, and folds.

4. Geomorphic evidence confirms active deformation.

Data Availability

Data are available upon request from the corresponding author.

Conflict of Interest

The authors declare no competing interests.

References

1) Abdikan, S., Sanli, F.B., Ustuner, M., Calò, F., 2016. Backscatter analysis using multi-temporal Sentinel-1 SAR data for monitoring crop growth of maize in Konya Basin, Turkey. The International Archives of the Photogrammetry, Remote Sensing and Spatial Information Sciences XLI-B8, 9–15.

2) Ahmed, T., Rehman, K., Shafique, M., Ali, W., 2023. GIS-based earthquake potential analysis in Northwest Himalayan, Pakistan. Environmental Earth Sciences 82(5), 113.

3) Ahmadi, H., Kalkan, K., Pekkan, E., 2023. Automatic lineaments detection using radar and optical data with an emphasis on geologic and tectonic implications: a case study of Kabul Block, eastern Afghanistan. Geocarto International, 2231400.

4) Aoki, T., et al., 2008. DEM generation using PALSAR data: Application to regional topographic mapping. ISPRS Journal of Photogrammetry and Remote Sensing 63(5), 554-567.

5) Baig, M.S., Khan, M.A., 2010. Active tectonics of the Kaghan Valley, Pakistan. Geol. Bull. Univ. Peshawar 43, 23–34.

6) Baig, M.S., Lawrence, R.D., 1987. Precambrian to Early Paleozoic orogenesis in the Himalaya. Tectonophysics 134(1–3), 1–14.

7) Bhosle, B., Parkash, B., Acharaya, P., 2009. Comparison of digital image processing techniques for lineament extraction using Landsat and SAR data in Raisen district, Madhya Pradesh, Central India. Journal of the Indian Society of Remote Sensing 37, 189-197.

8) Bilham, R., 2019. Himalayan earthquakes: a review of historical seismicity and early 21st century slip potential. Geological Society, London, Special Publications 483(1), 423-482.

9) Bovenga, F., et al., 2014. Application of multi-temporal differential interferometry to slope instability detection in urban/peri-urban areas. Engineering Geology 184, 57-70.

10) EL-Omairi, A., et al., 2024. Geomorphic analysis of fault activity in the High Atlas Mountains. Tectonophysics 850, 229752.

11) Ghosh, S., Philip, G., Prasad, A., Syed, T.H., Mohanty, S., 2023. Towards quantifying the relative tectonic activity in the Trans-Yamuna segment of NW Himalaya. Geocarto International, 2155712.

12) Huang, J., et al., 2017. Terrain correction for Sentinel-1 SAR data. Remote Sensing of Environment 196, 32-46.

13) Huang, X., et al., 2022. VH polarization for vegetation analysis in Himalayas. IEEE Transactions on Geoscience and Remote Sensing 60, 1-12.

14) Hu, X., Zhu, J., 2022. Back-thrust identification using SAR in NW Himalaya. Journal of Geophysical Research: Solid Earth 127(4), e2021JB023456.

15) Jiang, Z., et al., 2008. Monitoring of crustal deformation in the Tibetan Plateau using ALOS PALSAR data. Remote Sensing of Environment 112(11), 3664-3674.

16) Ji, Y., et al., 2020. Roughness index using VH polarization in mountainous regions. Remote Sensing 12(14), 2285.

17) Karaca, S.O., Abir, I.A., Khan, S.D., Ozsayın, E., Qureshi, K.A., 2021. Neotectonics of the

Western Suleiman Fold Belt, Pakistan: Evidence for Bookshelf Faulting. Remote Sensing 13(18), 3593.

18) Kazmi, A.H., Rana, R.A., 1982. Tectonic Map of Pakistan. Geological Survey of Pakistan.

19) Kwak, Y., et al., 2007. PALSAR data characteristics for deformation monitoring. IEEE Geoscience and Remote Sensing Letters 4(3), 457-461.

20) Latif, M.A., 1970. Explanatory notes on the geology of southeastern Hazara to accompany the revised geological map. Jahrbuch der Geologischen Bundesanstalt 15, 5-11.

21) Liu, X., Zhao, C., Zhang, Q., Lu, Z., Li, Z., Yang, C., Zhu, W., Liu-Zeng, J., Chen, L., Liu, C., 2021. Integration of Sentinel-1 and ALOS/PALSAR-2 SAR datasets for mapping active landslides along the Jinsha River corridor, China. Engineering Geology 284, 106033.

22) Lu, Z., et al., 2007. InSAR detection of coseismic and postseismic displacements caused by the 2001 Geiyo earthquake in Japan. Journal of Geophysical Research: Solid Earth 112(B11), B11405.

23) Lu, Z., et al., 2021. Advances in SAR applications for tectonic studies. Remote Sensing of Environment 264, 112584.

24) Mahmood, S.A., Batool, H., Waheed, Z., Akhtar, A.M., Masood, A., 2013. Investigation of Neotectonics along Hazara Kashmir Syntaxis through Remote Sensing and GIS Analysis. International Journal of Recent Development in Engineering and Technology 1(3), 61-67.

25) Mahmood, S.A., Yameen, M., Sheikh, R.A., Rafique, H.M., Almas, A.S., 2012. DEM and GIS based hypsometric analysis to investigate neotectonic influence on Hazara Kashmir Syntaxis. Pakistan Journal of Science 64(3), 209-213.

26) Meixner, J., et al., 2018. Fault-controlled drainage in Himalayas. Geomorphology 305, 112-124.

27) Oguchi, T., et al., 2003. Stream patterns controlled by faults in Japan. Geomorphology 51(1-3), 29-45.

28) Oludare, O.I., Kazeem, R.A., Shaibayo, A.S., Awonusi, A.A., Dare, A.A., Ikumapayi, O.M., Adaramola, B.A., 2023. An Assessment of Earthquake-Induced Landslides Distribution in Nepal Using Open-Source Applications on Sentinel-1 Tops SAR Imagery. International Journal of Design & Nature and Ecodynamics 18(2), 237-249.

29) Rather, A.A., Bukhari, S.K., 2025. Interseismic deformation and 3D kinematic reconstruction of the Balapur Fault, NW Himalaya: Insights from InSAR and gravity data. Tectonophysics 907, 230744.

30) Saraf, A.K., et al., 2002. Satellite data utilization for fault mapping in Himalayas. International Journal of Remote Sensing 23(21), 4583-4594.

31) Shahzad, F., Gloaguen, R., 2011. TecDEM: A MATLAB based toolbox for tectonic geomorphology, Part 2: Surface dynamics and basin analysis. Computers & Geosciences 37(2), 261-271.

32) Shami, P.A., Baig, M.S., 2002. Structural evolution of the Himalayan foothills, northern Pakistan. Journal of Asian Earth Sciences 20(8), 913–927.

33) Shimada, M., et al., 2009. ALOS PALSAR radiometric and geometric calibration. IEEE

Transactions on Geoscience and Remote Sensing 47(12), 3915–3932.

34) Small, D., Schubert, A., 2019. Guide to Sentinel-1 interferometric wide-swath data processing. Remote Sensing 11(20), 2339.

35) Thollard, F., et al., 2021. Terrain flattening effects on Sentinel-1 data. Remote Sensing 13(5), 987.

36) Wadia, D.N., 1928. The Geology of India. Macmillan, London.

37) Waheed, Z., Batool, S., Amer, A., Mehmood, S.A., Arif, H., Aslam, R.M.S., Shahzad, M., Talib, B., 2019. Remote Sensing and Morphotectonic Analysis in Hazara Kashmir Syntaxis Using River Longitudinal Profiles. International Journal of Innovations in Science & Technology 3(1), 179-191.

38) Watson, C.S., et al., 2022. VH polarization for roughness studies in Himalayas. Earth Surface Processes and Landforms 47(5), 1234-1245.

39) Weilert, T., Laó-Dávila, D.A., 2023. Fault-controlled streams in Puerto Rico. Tectonics 42(2), e2022TC007456.

40) Xiong, S., Muller, J.-P., Li, G., 2017. The application of ALOS/PALSAR InSAR to measure subsurface penetration depths in deserts. Remote Sensing 9(6), 638.

41) Yin, A., 2006. Cenozoic tectonic evolution of the Himalayan orogen as constrained by along-strike variation of structural geometry, exhumation history, and foreland sedimentation. Earth-Science Reviews 76(1-2), 1-131.

42) Zeinalov, G.A., et al., 2000. Remote sensing in structural geology. Journal of Petroleum Geology 23(4), 457-472.

43) Zhang, L., et al., 2019. Resolution limitations in PALSAR data for deformation monitoring. Remote Sensing 11(7), 845.

44) Zhao, C., Liang, J., Zhang, S., Dong, J., Yan, S., Yang, L., Liu, B., Ma, X., Li, W., 2022. Integration of Sentinel-1A, ALOS-2 and GF-1 Datasets for Identifying Landslides in the Three Parallel Rivers Region, China. Remote Sensing 14(19), 5031.

45) Zhou, X., et al., 2015. PALSAR applications in urban deformation monitoring. IEEE Journal of Selected Topics in Applied Earth Observations and Remote Sensing 8(4), 1702-1712.

46) Zhu, J., et al., 2022. Multidimensional terrain analysis using SAR. Geomorphology 399, 108056.